Acta Polytechnica **62**(4):479–487, 2022
https://doi.org/10.14311/AP.2022.62.0479

Published by the Czech Technical University in Prague

ACTIVE DISTURBANCE REJECTION CONTROL-BASED ANTI-COUPLING METHOD FOR CONICAL MAGNETIC BEARINGS

Danh Huy Nguyen[a], Minh Le Vu[a], Hieu Do Trong[a], Danh Giang Nguyen[b], Tung Lam Nguyen[a,*]

[a] *Hanoi University of Science and Technology, School of Electrical Engineering, 1 Dai Co Viet st, Hanoi 100000, Vietnam*

[b] *National University of Civil Engineering, Faculty of Mechanical Engineering, 55 Giai Phong st, Hanoi 100000, Vietnam*

[*] corresponding author: lam.nguyentung@hust.edu.vn

Abstract. Conical-shape magnetic bearings are currently a potential candidate for various magnetic force-supported applications due to their unique geometric nature reducing the number of required active magnets. However, the bearing structure places control-engineering related problems in view of underactuated and coupling phenomena. The paper proposes an Adaptive Disturbance Rejection Control (ADRC) for solving the above-mentioned problem in the conical magnetic bearing. At first, virtual current controls are identified to decouple the electrical sub-system, then the active disturbance rejection control is employed to eliminate coupling effects owing to rotational motions. Comprehensive simulations are provided to illustrate the control ability.

Keywords: Conical active magnetic bearings, over-actuated systems, ADRC, coupling mechanism, linearization.

1. Introduction

Recently, active magnetic bearing (AMB) has been of increasing interest to the manufacturing industry due to its contactless, lubrication-free, no mechanical wear, and high-speed capability [1–3]. These characteristics enable them to be employed in a variety of applications, including artificial hearts [4], vacuum pumps [5], and flywheel energy storage systems [6] and [7], etc. The motion resolution of the suspended object in translation or high-speed rotation is restricted solely by the actuators, sensors, and the servo system utilised due to the non-contact nature of a magnetic suspension. As a result, magnetic bearings can be utilised in almost any environment as long as the electromagnetic parts are suitably shielded, for example, in open air at temperatures ranging from 235 °C to 450 °C [8]. Many researchers, in particular, have endeavored to design a range of AMBs that are compact and simple-structured while still performing well. Because of the advantages of a cone-shaped active magnetic bearing (AMB) system, such as its simple structure, low heating, and high dependability, there is an increasing number of studies on it [9, 10]. The structure of a conical magnetic bearing is identical to that of a regular radial magnetic bearing, with the exception that both the stator and rotor working surfaces are conical, allowing force to be applied in both axial and radial directions [11, 12]. The conical form saves axial space, which can be used to install gears and other components for an added mechanical benefit. It also conserves energy for an optimal load support. Conical electromagnetic bearings feature two coupled properties as compared to ordinary radial electromagnetic bearings: current-coupled and geometry-coupled effects, making dynamic modelling and control of these systems particularly difficult. The current-coupled effect exists because the axial and radial control currents flow in the bearing coils simultaneously. Furthermore, the inclined angle of the magnet core causes a geometry-coupled effect. Coupled dynamic characteristics of the rotor conical magnetic bearing system became known due to the existence of the two coupled effects. So far, several researchers have discussed the modelling and control of cone-shaped AMBs [2, 13, 14]. Lee CW and Jeong HS presented a control method for conical magnetic bearings in [12], which allows the rotor to float in the air stably. They proposed a completely connected linearised dynamic model for the cone-shaped magnet coil that covers the relationships between the input voltage and output current. The connected controller uses a linear quadratic regulator with integral action to stabilise the AMB system, while the decoupled controller is used to stabilise the five single DOF systems. Abdelfatah M. Mohamed et al. [11] proposed the Q-parameterization method for designing system stabilisation in terms of two free parameters. The proposed technique is validated using a digital simulation. As a result, plant parameters such as transient and forced response are good, and stiffness characteristics are obtained with small oscillation. Recently, in [15], E. E. Ovsyannikova and A. M. Gus'kov cre-

ated a mathematical model of a rigid rotor suspended in a blood flow and supported by conical active magnetic bearings. They used the proportional-integral differential (PID) control, which takes into account the influence of hydrodynamic moments, which affect the rotor from the side of the blood flow, as well as external influences on the person. The experimental findings are reported, with a rotor speed range of 5000 to 12000 rpm and a placement error of less than 0.2 mm. Nguyen et al. introduced a control approach considering input and output constraints in the magnetic bearing system in [16] and [17]. The control restricts the rotor displacement in a certain range according to the system structure. In [18], modelling of a conical AMB structure for a complete support of 5-dof rotor system was reported by A. Katyayn and P. K. Agarwal, who improved the system's performance by creating the Interval type-2 fuzzy logic controller (IT2FLC) with an uncertain bound algorithm. This controller reduces the need for a precise system modeling while also allowing for the handling of parameter uncertainty. The simulation results show that the proposed controller outperforms the type-1 fuzzy logic controller in terms of transient responses.

In this paper, we examine the concept of conical magnetic bearings for both the radial and axial displacement control. The governing equations characterising the relationship between magnetic forces, air gaps, gyroscopic force, and control currents are used to build the nonlinear model of the conical magnetic bearing. The main contribution of the paper is that rotational motions are treated as disturbances and are handled by the Active Disturbance Rejection Control (ADRC) [19, 20] to stabilise the cone-shaped AMB system. ADRC was developed as an option that combines the easy applicability of conventional PID-type control methods with the strength of modern model-based approaches. The core of ADRC is an extended observer that treats actual disturbances and modelling uncertainty together, using only a very coarse process model to create a control loop. Because of the excellent abilities of ADRC, the paper also tackles the unwanted dynamics due to rotational motions, which are normally neglected in other related works. The ignorance might lead to system degradation due to a high operating speed resulting in strong coupling effects. The effectiveness of the proposed control structure for stabilising the rotor position and rejecting coupling-phenomenon-induced disturbance is numerically evaluated through comprehensive scenarios.

2. Dynamic modelling of conical magnetic bearings

Consider the simplified model of a conical magnetic bearing system as shown in Fig. 1. It is assumed that the rotor is rigid and its centre of mass and geometric centre are coincide. Furthermore, the assumptions of non-saturated circuit and negligible flux linkage between magnetic coils are made. R_m and β are the

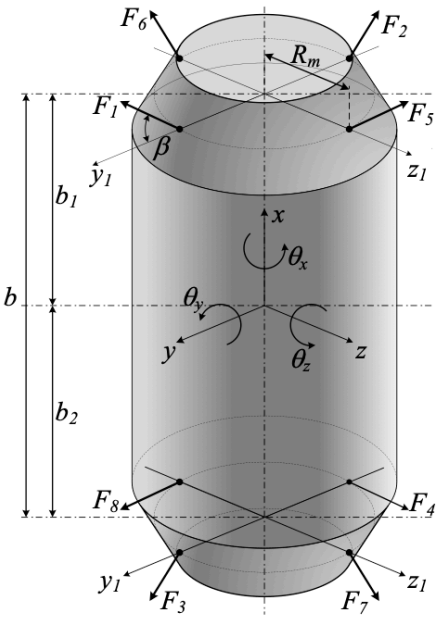

Figure 1. Model of a cone-shaped active magnetic bearing system.

effective radius and inclined angle of the magnetic core, b_1 and b_2 are the distances between the two radical magnetic bearing and the centre of gravity of the rotor; F_j (j =1 to 8) are the magnetic forces produced by the stator and exerted on the rotor; (x, y, z) and $(\theta_x, \theta_y, \theta_z)$ are the displacement and angular coordinates defined with respect to the centre of mass. The cone-shaped active magnetic bearing system can be modelled as follows:

$$\begin{aligned}
m\ddot{x} &= (F_1 + F_2 + F_5 + F_6)\sin\beta \\
&\quad - (F_3 + F_4 + F_7 + F_8)\sin\beta - mg. \\
m\ddot{y} &= (F_1 - F_2 + F_3 - F_4)cos\beta. \\
m\ddot{z} &= (F_5 - F_6 + F_7 - F_8)cos\beta. \\
J_d\ddot{\theta}_y &= [(F_6 - F_5)b_1 + (F_7 - F_8)b_2]\cos\beta \\
&\quad + (F_5 - F_6 + F_8 - F_7)R_m\sin\beta + J\dot{\theta}_x\dot{\theta}_z. \\
J_d\ddot{\theta}_z &= [(F_1 - F_2)b_1 + (F_4 - F_3)b_2]\cos\beta \\
&\quad + (F_2 - F_1 + F_3 - F_4)R_m\sin\beta + J\dot{\theta}_x\dot{\theta}_y
\end{aligned} \tag{1}$$

where J is the moment of inertia of the rotor about the axis of rotation. The mass and moment of inertia of the rotor are m and J_d, respectively. We also consider the effect of the x-axis rotation on the other two axes.

Here, the first three equations in Eq. (1) are the kinematics of the rotor's transverse motion, while the last two equations represent the rotor's rotational dynamics. In addition, in the two rotational kinematics equations, there is an additional component of the feedback force. Suppose that when the rotor rotates rapidly if a force is applied to the y-axis (z-axis) that is sufficiently large to deflect the rotor from the axis of motion by a small angle, the rotor itself will also react back to a torque of the corresponding magnitude equal to $J\dot{\theta}_x\dot{\theta}_z$. Similarly, the component of gyro force

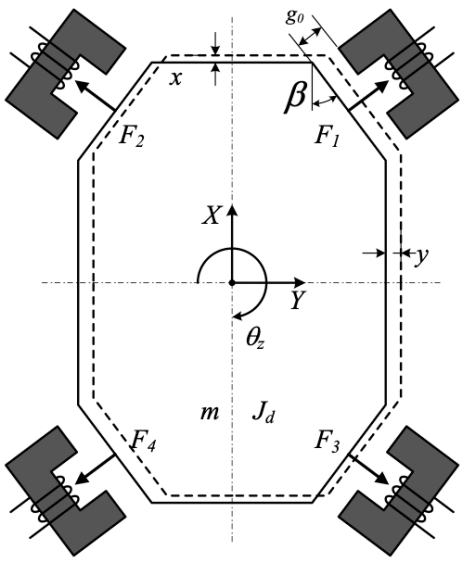

FIGURE 2. Simplified model of the cone-shaped AMB system.

along the z-axis is computed. In order to linearise, the dynamic equation (1), small motions of the rotor are considered. Fig. 2 shows the change of the air gap of the cone-shaped magnet, which is written as:

$$\begin{aligned} g_{y_{1,2}} &= g_o - x\sin\beta \pm (y + b_1\theta_z)\cos\beta \\ g_{y_{3,4}} &= g_o + x\sin\beta \pm (y - b_2\theta_z)\cos\beta \\ g_{z_{1,2}} &= g_o - x\sin\beta \pm (z + b_1\theta_y)\cos\beta \\ g_{z_{3,4}} &= g_o + x\sin\beta \pm (z + b_2\theta_y)\cos\beta \end{aligned} \tag{2}$$

where g_o is the steady-state nominal air gap. The magnetic force can be written regrading to he actual air gap and the current as:

$$\begin{aligned} F_{1,2} &= \frac{\mu_o A_p N^2 (I_{o_1} + i_{y_{1,2}})^2}{4{g_{y_{1,2}}}^2} \\ F_{3,4} &= \frac{\mu_o A_p N^2 (I_{o_2} + i_{y_{3,4}})^2}{4{g_{y_{3,4}}}^2} \\ F_{5,6} &= \frac{\mu_o A_p N^2 (I_{o_1} + i_{z_{1,2}})^2}{4{g_{z_{1,2}}}^2} \\ F_{7,8} &= \frac{\mu_o A_p N^2 (I_{o_2} + i_{z_{3,4}})^2}{4{g_{z_{3,4}}}^2} \end{aligned} \tag{3}$$

where $\mu_o (= 4\pi \times 10^{-7} H/m)$ is the permeability of free space; $A_p = A/cos\beta$, A is the cross-sectional area, N is the number of coil turns; $i_{q_j} (j = \overline{1,4} \& q = y, z)$ is the control current of each magnet; I_{o_1} and I_{o_2} are the bias currents in the upper and lower bearing. Assume that the current change and the displacement of the rotor are small relative to the bias current I_o and the nominal air gap. Apply Eq. (2) to Eq. (3) and use the Taylor expansion series to obtain the magnetic force, which is linearised as:

$$\begin{aligned} F_{1,2} &= F_{o_1} + K_{i_1} i_{y_{1,2}} + K_{q_1} x\sin\beta \\ &\quad \pm K_{q_1}(y + b_1\theta_z)\cos\beta \\ F_{3,4} &= F_{o_2} + K_{i_2} i_{y_{3,4}} + K_{q_2} x\sin\beta \\ &\quad \pm K_{q_2}(y - b_2\theta_z)\cos\beta \\ F_{5,6} &= F_{o_1} + K_{i_1} i_{z_{1,2}} + K_{q_1} x\sin\beta \\ &\quad \pm K_{q_1}(z - b_1\theta_y)\cos\beta \\ F_{7,8} &= F_{o_2} + K_{i_2} i_{z_{3,4}} + K_{q_2} x\sin\beta \\ &\quad \pm K_{q_2}(z + b_2\theta_y)\cos\beta \end{aligned} \tag{4}$$

where $F_{oj} = \frac{\mu_o A_p N^2 {I_{oj}}^2}{4{g_o}^2}, j = 1, 2$ are the steady-state magnetic forces and $k_{qj} = \frac{2F_{oj}}{g_o}, k_{ij} = \frac{2F_{oj}}{I_{oj}}, j = 1, 2$ are the position and current stiffnesses, respectively.

From the combination of Eqs. (1) and (4), the linear differential equation showing the kinematics of the 5 degrees of freedom conical-AMB drive system can be rewritten as:

$$\mathbf{M}_b \ddot{\mathbf{q}}_b + \mathbf{K}_b \mathbf{q}_b = \mathbf{K}_{ibm} \mathbf{i}_m + G\dot{\mathbf{q}}_b \tag{5}$$

where

$$\mathbf{q}_b = \{\, x, y, z, \theta_y, \theta_z \,\}^{\,T}$$

$$\mathbf{i}_m = \{\, i_{y_1}, i_{y_2}, i_{y_3}, i_{y_4}, i_{z_1}, i_{z_2}, i_{z_3}, i_{z_4} \,\}^{\,T}$$

$$\mathbf{K}_b = \begin{bmatrix} -K_{xx} & 0 & 0 & 0 & 0 \\ 0 & -K_{yy} & 0 & 0 & -K_{y\theta_z} \\ 0 & 0 & -K_{zz} & -K_{z\theta_y} & 0 \\ 0 & 0 & -K_{\theta_y z} & -K_{\theta_y\theta_y} & 0 \\ 0 & -K_{\theta_z y} & 0 & -K_{\theta_z\theta_z} & 0 \end{bmatrix}$$

$$G = \begin{bmatrix} 0 & 0 & 0 & 0 & 0 \\ 0 & 0 & 0 & 0 & 0 \\ 0 & 0 & 0 & 0 & 0 \\ 0 & 0 & 0 & 0 & J\dot{\theta_x} \\ 0 & 0 & 0 & J\dot{\theta_x} & 0 \end{bmatrix}$$

$$\mathbf{K}_{ibm} = \begin{bmatrix} K_{i_1}\mathrm{S}\beta & K_{i_1}\mathrm{C}\beta & 0 & 0 & K_{i_1}\sigma \\ K_{i_1}\mathrm{S}\beta & -K_{i_1}\mathrm{C}\beta & 0 & 0 & -K_{i_1}\sigma \\ -K_{i_2}\mathrm{S}\beta & K_{i_2}\mathrm{C}\beta & 0 & 0 & K_{i_2}\gamma \\ -K_{i_2}\mathrm{S}\beta & -K_{i_2}\mathrm{C}\beta & 0 & 0 & -K_{i_2}\gamma \\ K_{i_1}\mathrm{S}\beta & 0 & K_{i_1}\mathrm{C}\beta & K_{i_1}\alpha & 0 \\ K_{i_1}\mathrm{S}\beta & 0 & -K_{i_1}\mathrm{C}\beta & -K_{i_1}\alpha & 0 \\ -K_{i_2}\mathrm{S}\beta & 0 & K_{i_2}\mathrm{C}\beta & K_{i_2}\gamma & 0 \\ -K_{i_2}\mathrm{S}\beta & 0 & -K_{i_2}\mathrm{C}\beta & -K_{i_2}\gamma & 0 \end{bmatrix}$$

$$\mathbf{M}_b = \begin{bmatrix} m & 0 & 0 & 0 & 0 \\ 0 & m & 0 & 0 & 0 \\ 0 & 0 & m & 0 & 0 \\ 0 & 0 & 0 & J_d & 0 \\ 0 & 0 & 0 & 0 & J_d \end{bmatrix}$$

$$K_{xx} = 4\,(K_{q_1} + K_{q_2})\,\mathrm{S}^2\beta$$

$$K_{yy} = K_{zz} = 2\mathrm{C}^2\beta\,(K_{q_1} + K_{q_2})$$

$$K_{y\theta_z} = K_{z\theta_y} = 2\mathrm{C}^2\beta\,(K_{q_1} b_1 + K_{q_2} b_2)$$

$$
\begin{aligned}
K_{\theta_y z} &= 2\mathrm{C}^2\beta\left(K_{q_1}b_1 + K_{q_2}b_2\right) \\
&\quad + \mathrm{S}(2\beta)R_m\left(K_{q_1} - K_{q_2}\right) \\
K_{\theta_z y} &= 2\mathrm{C}^2\beta\left(K_{q_1}b_1 - K_{q_2}b_2\right) \\
&\quad - \mathrm{S}(2\beta)R_m\left(K_{q_1} - K_{q_2}\right) \\
K_{\theta_y\theta_y} &= 2\mathrm{C}^2\beta\left(K_{q_1}{b_1}^2 - K_{q_2}{b_2}^2\right) \\
&\quad + \mathrm{S}(2\beta)R_m\left(K_{q_1}b_1 + K_{q_2}b_2\right) \\
K_{\theta_z\theta_z} &= 2\mathrm{C}^2\beta\left(K_{q_1}{b_1}^2 + K_{q_2}{b_2}^2\right) \\
&\quad - \mathrm{S}(2\beta)R_m\left(K_{q_1}b_1 + K_{q_2}b_2\right) \\
\alpha &= b_1\mathrm{C}\beta + R_m\mathrm{S}\beta; \sigma = b_1\mathrm{C}\beta - R_m\mathrm{S}\beta \\
\gamma &= b_2\mathrm{C}\beta - R_m\mathrm{S}\ \beta
\end{aligned}
$$

Here, $\mathbf{q}_b$ is the displacement vector defined in the mass centre coordinates; $\mathbf{i}_m$ is the control current vector and $\mathbf{M}_b$, $\mathbf{K}_b$ and $\mathbf{K}_{ibm}$ are the mass, position stiffness, and current stiffness matrices, respectively. As can be observed, the system's equation is complicated and coupled because the components outside the main diagonal of the matrices, $\mathbf{K}_b$, $\mathbf{K}_{ibm}$ and $\mathbf{G}$ are non-zero. Due to this characteristic, conventional linear control rules cannot be applied directly to each motion direction. As a result, the Active Disturbance Rejection Control (ADRC) algorithm is employed to handle the coupling effects by taking these effects as system disturbances.

3. Control system design

The conical AMB system is naturally unstable, a closed-loop control is required to stabilise the rotor position. The control current of the system can be calculated through the control structure "different driving mode", which is shown in Fig. 3.

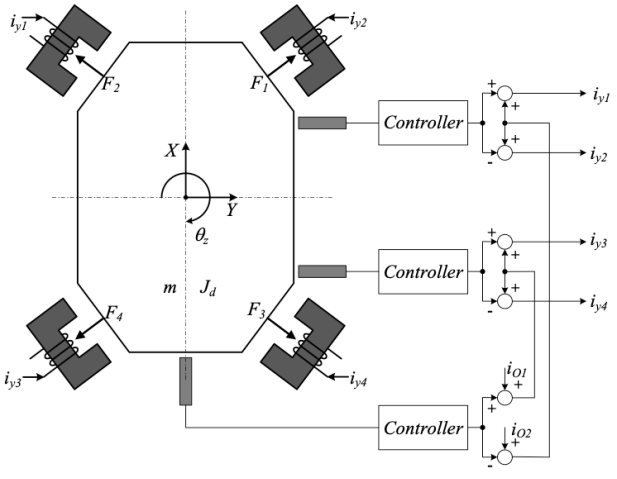

Figure 3. Conceptual control loop of the cone-shaped active magnetic bearings.

The main principle of the aforementioned structure: where controlling the position of the rotor according to the $Y-axis$ and $Z-axis$, the magnet pairs are in the poles that are opposite each other. For example, i_{y_1} and i_{y_2} magnets, as well as, i_{y_3} and i_{y_4}, i_{z_1} and i_{z_2}, i_{z_3} and i_{z_4} are similarly controlled by this structure. Here, the magnet in each pair is controlled by the sum of the bias current and control current, and the other with the difference of the bias current and control current. This means that when the rotor is displaced from its equilibrium position, the "different driving mode" controls the pairs of magnets, whereas when the rotor is in its equilibrium position, only the bias current is present on each pair of the magnets. When the rotor deviates from the equilibrium position, the current through the pairs of magnets is written as in the following equation:

$$
\begin{bmatrix} i_{y_1} \\ i_{y_2} \\ i_{y_3} \\ i_{y_4} \\ i_{z_1} \\ i_{z_2} \\ i_{z_3} \\ i_{z_4} \end{bmatrix} = \begin{bmatrix} I_{o_1} \\ I_{o_1} \\ I_{o_2} \\ I_{o_2} \\ I_{o_1} \\ I_{o_1} \\ I_{o_2} \\ I_{o_2} \end{bmatrix} + \begin{bmatrix} 1 & 0 & 0 & 0 & -1 \\ -1 & 0 & 0 & 0 & -1 \\ 0 & 1 & 0 & 0 & 1 \\ 0 & -1 & 0 & 0 & 1 \\ 0 & 0 & 1 & 0 & -1 \\ 0 & 0 & 0 & -1 & -1 \\ 0 & 0 & 0 & 1 & 1 \\ 0 & 0 & 0 & -1 & 1 \end{bmatrix} \begin{bmatrix} I_{yt} \\ I_{yd} \\ I_{zt} \\ I_{zd} \\ I_x \end{bmatrix} \tag{6}
$$

where $\mathbf{I}_o = [I_{o_1}, I_{o_1}, I_{o_2}, I_{o_2}, I_{o_1}, I_{o_1}, I_{o_2}, I_{o_2}]^T$ is the bias current. At steady-state, consider $\mathbf{I}_o = 0$, $\mathbf{i}_r = [I_{yt}, I_{yd}, I_{zt}, I_{zd}, I_x]^T$ is the x, y, and z axes' virtual control current. I_x is the virtual control current of x-axes. The virtual control current in the upper half of the y and z axes is (I_{yt}, I_{zt}) , whereas the virtual control current in the bottom half is (I_{yd}, I_{zd}).

$$
\mathbf{H} = \begin{bmatrix} 1 & -1 & 0 & 0 & 0 & 0 & 0 & 0 \\ 0 & 0 & 1 & -1 & 0 & 0 & 0 & 0 \\ 0 & 0 & 0 & 0 & 1 & 0 & 0 & 0 \\ 0 & 0 & 0 & 0 & 0 & -1 & 1 & -1 \\ -1 & -1 & 1 & 1 & -1 & -1 & 1 & 1 \end{bmatrix}^T
$$

In this case, Eq. (5) can be rewritten as:

$$
\mathbf{M}_b\ddot{\mathbf{q}}_b - \mathbf{G}\dot{\mathbf{q}}_b + \mathbf{K}_b\mathbf{q}_b = \mathbf{K}_{ibm}\mathbf{H}\mathbf{i}_r \tag{7}
$$

Since the control is performed in the bearing coordinates, rewriting the equations of motion in bearing coordinates utilising the relationship between the mass-centre coordinates $(x, y, z, \theta_y, \theta_z)$ and the bearing coordinates (x, y_1, y_2, z_1, z_2), given by:
$\mathbf{q}_b = \{\ x, y, z, \theta_y, \theta_z\}^T$ and $\mathbf{q}_{se} = \{\ x, y_1, y_2, z_1, z_2\}^T$
$\mathbf{q}_{se} = \mathbf{T}\mathbf{q}_b$ with $\mathbf{T}$ is the coordinate transfer matrix

$$
\mathbf{T} = \begin{bmatrix} 1 & 0 & 0 & 0 & 0 \\ 0 & 1 & 0 & 0 & b_1 \\ 0 & 1 & 0 & 0 & -b_2 \\ 0 & 0 & 1 & -b_1 & 0 \\ 0 & 0 & 1 & b_2 & 0 \end{bmatrix}
$$

Eq. (1) shows that the inter-channel effect occurs at $\mathbf{K}_b$ and $\mathbf{K}_{ibm}\mathbf{H}$ because the major non-diagonal components are not zero. The $\mathbf{K}_b$ and $\mathbf{K}_{ibm}\mathbf{H}$ are invertible. The following control structure is used to eliminate the interstitial component:

$$
\mathbf{i}_r = (\mathbf{K}_{ibm}\mathbf{H})^{-1}(\mathbf{v} + \mathbf{K}_b\mathbf{T}^{-1}\mathbf{q}_{se}) \tag{8}
$$

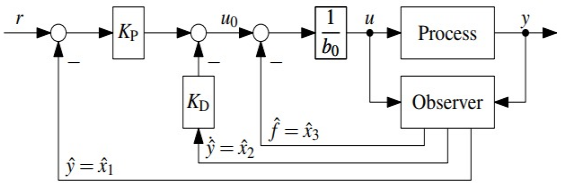

FIGURE 4. Control loop structure with active disturbance rejection control (ADRC).

Eq. (7) can be rewritten as:

$$\mathbf{M}_b\ddot{\mathbf{q}}_b - \mathbf{G}\dot{\mathbf{q}}_b = \mathbf{v} \tag{9}$$

where $\mathbf{v}$ is the new control signal's vector. The interstitial component has been removed in the control channels (x, y, z) leaving just the interstitial component in the control channel (θ_y, θ_z) owing to the gyroscope force.

The original model of the magnetic bearing is a complex, multivariable nonlinear system, through the process of linearity and decoupling, we have the linear form of the system shown in Eq. (9) with 5 inputs and 5 outputs. The full form of Eq. (9) is shown as follows:

$$\begin{cases} m\,\ddot{x} = v_1 \\ m\,\ddot{y} = v_2 \\ m\,\ddot{z} = v_3 \\ J_d\,\ddot{\theta}_y + J\,\dot{\theta}_x\,\dot{\theta}_z = v_4 \\ J_d\,\ddot{\theta}_z + J\,\dot{\theta}_x\,\dot{\theta}_y = v_5 \end{cases} \tag{10}$$

Remark: It is noted that the first three equations of Eq. (10) characterise the transnational motions and can be readily stabilized using v_1, v_2, and v_3. The last two equation indicate coupling mechanism related to the rotational motion of the rotor that is normally ignored. In practice, the magnetic bearing is normally employed to operate in high speed range, hence rotational motion effects can not be neglected.

In this section, the ADRC controller will be used to remove the remaining coupling components as well as to stabilise the control object. An ADRC controller is used for each input and output pair $(x, v_1), (y, v_2), (z, v_3), (\theta_y, v_4), (\theta_z, v_5)$. In ADRC design, $f(t)$ is unknown and is considered as a "generalized disturbance", and b_0 is the available information concerning the model. The according structure of the control loop with ADRC is presented in Fig. 4. The fundamental idea of ADRC is to implement an extended state observer (ESO) that provides an estimate, $\hat{f}(t)$, such that we can compensate the impact of $f(t)$ on our system. The equation for the extended state observer is given as:

$$\begin{aligned} \begin{pmatrix} \dot{\hat{x}}_1(t) \\ \dot{\hat{x}}_2(t) \\ \dot{\hat{x}}_3(t) \end{pmatrix} &= \begin{pmatrix} 0 & 1 & 0 \\ 0 & 0 & 1 \\ 0 & 0 & 0 \end{pmatrix} \begin{pmatrix} \hat{x}_1(t) \\ \hat{x}_2(t) \\ \hat{x}_3(t) \end{pmatrix} \\ &+ \begin{pmatrix} 0 \\ b_0 \\ 0 \end{pmatrix} u(t) + \begin{pmatrix} l_1 \\ l_2 \\ l_3 \end{pmatrix} (y(t) - \hat{x}_1(t)) \\ &= \underbrace{\begin{pmatrix} -l_1 & 1 & 0 \\ -l_2 & 0 & 1 \\ -l_3 & 0 & 0 \end{pmatrix}}_{A-LC} \begin{pmatrix} \hat{x}_1(t) \\ \hat{x}_2(t) \\ \hat{x}_3(t) \end{pmatrix} \\ &+ \underbrace{\begin{pmatrix} 0 \\ b_0 \\ 0 \end{pmatrix}}_{B} u(t) + \begin{pmatrix} l_1 \\ l_2 \\ l_3 \end{pmatrix} y(t) \end{aligned} \tag{11}$$

where $\hat{x}_1(t) = \hat{y}(t)$; $\hat{x}_2(t) = \dot{\hat{y}}(t)$; $\hat{x}_3(t) = \hat{f}(t)$. Removing the unknown components is done through the following control law:

$$\begin{aligned} \ddot{y}(t) &= (f(t) - \hat{f}(t)) + u_0(t) \approx u_0(t) \\ &\approx K_P.((r(t) - y(t)) - K_D.\dot{y}(t)) \end{aligned} \tag{12}$$

where r is the setpoint. In order to work properly, observer parameters, l_1, l_2, l_3, in Eq. (11) still have to be determined. According to [20], the ADRC's parameters can be chosen to tune the closed-loop to a critically damped behaviour and a desired 2% settling time T_{settle}. The tuning procedure is summarised as follows:

$$\begin{aligned} K_p &= \left(s^{CL}\right)^2, K_D = -2.s^{CL} \\ l_1 &= -3.s^{ESO}, l_2 = 3.\left(s^{ESO}\right)^2, l_3 = \left(s^{ESO}\right)^3 \end{aligned} \tag{13}$$

with $s^{CL} = -\frac{6}{T_{settle}}$ being the negative-real double closed-loop pole.

$s^{ESO} \approx (3...10).s^{CL}$ is the observer pole. Using the ADRC controller to calculate the variable x, y and z are calculated similarly:

$$\begin{aligned} \ddot{x} &= \underbrace{(\frac{1}{m}.d(t) + \Delta b.u(t))}_{f(t)} + b_{01}v_1 \\ &= f(t) + b_{01}.v_1(t) \\ v_1(t) &= K_{P1}.((r(t) - \hat{x}(t)) - K_{D1}.\dot{\hat{x}}(t)) \end{aligned} \tag{14}$$

For equations containing the two variables (θ_y and θ_z), which have an interleaved component between the two equations. Because the interleaved component is unknown, the extended observer can be used to estimate and analyse it, using the ADRC controller with variable θ_y, as follows:

$$\begin{aligned} \ddot{\theta}_y &= (\frac{1}{J}d(t) + \Delta b.v_4(t) + J\theta_x\theta z) + b_{04}v_4 \\ &= f(t) + b_{04}.v_4(t) \\ b_{04} &= \frac{1}{J} \\ v_4(t) &= K_{P4}.((r(t) - \hat{\theta}_y(t)) - K_{D4}.\dot{\hat{\theta}}_y(t)) \end{aligned} \tag{15}$$

Name	Symbol
$b_{01} = b_{02} = b_{03}$	$1/m$
$b_{04} = b_{05}$	$1/J$
T_{settle}	0.1 (s)
s^{CL}	-60
K_{Pi} $(i = 1, \ldots, 5)$	3600
K_{Di} $(i = 1, \ldots, 5)$	120
s^{ESO}	-420
l_{1i} $(i = 1, \ldots, 5)$	1260
l_{2i} $(i = 1, \ldots, 5)$	529200
l_{3i} $(i = 1, \ldots, 5)$	74088000

Table 1. Controller parameters.

4. NUMERICAL SIMULATIONS

In this section, we consider two scenarios to evaluate the effectiveness of using the ADRC controller in the case of variable speed rotation and rotor load disturbance.

Bearing design parameters	Value
Radial air gap g_0	0.5 mm
Cross-sectional area A	18*10 mm
Inclined angle β	10^o
Magnetic coils N	300 turns
Resistance R	2 Ω
Inductance of wire L_0	20 mH
Rotor mass M	1.86 Kg
Moment of inertia J_d	0.00647 kgm^2
Moment of inertia J_p	0.00121 kgm^2
Bias current I_{01}, I_{02}	1.6 A,1 A
Bearing span b_1, b_2	81.7 mm,71.6 mm

Table 2. System parameters.

4.1. Simulation scenario 1:

We design an ADRC controller with a rotor rotation speed of 3000 rpm. The initial values of the rotor's centre of mass position are: $x_0 = 0.25.10^{-3}; y_0 = 0.2.10^{-3}; z_0 = 0.125.10^{-3}; \theta_y = 0.1.10^{-3}; \theta_z = 0.2.10^{-3}$. Select the coefficients of the ADRC as follows $s^{CL} = -\frac{6}{0.1}, s^{ESO} = 7s^{CL}, K_P = (s^{CL})^2, K_D = -2s^{CL}, l_1 = -3s^{ESO}; l_2 = 3\left(s^{ESO}\right)^2, l_3 = -(s^{ESO})^3$.

The position of the centre of mass and the deflection angle of the rotor return to the equilibrium position after a time interval of 0.1 seconds and there is no overshoot in Fig. 5 and Fig. 6. From Fig. 7, initially, when the rotor position deviates from the equilibrium position, a control current is generated to bring the rotor back to the equilibrium position. After the rotor is in the equilibrium position, the control current is zero so that the bias currents I_{01} and I_{02} keep the rotor in this equilibrium state. The impact force of the magnet is shown in Fig. 8 as having a significant value

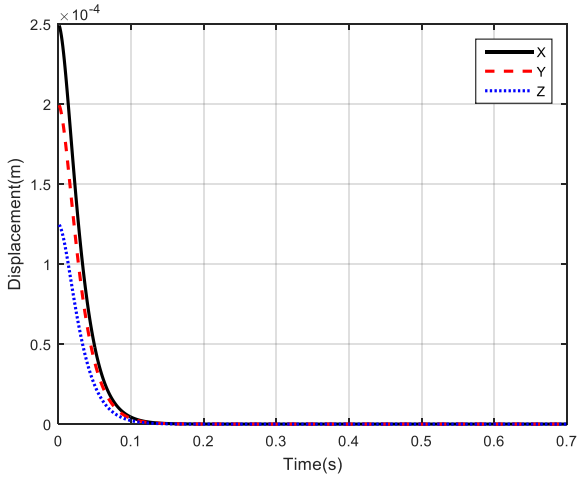

Figure 5. Response to the position of the x, y, z axes.

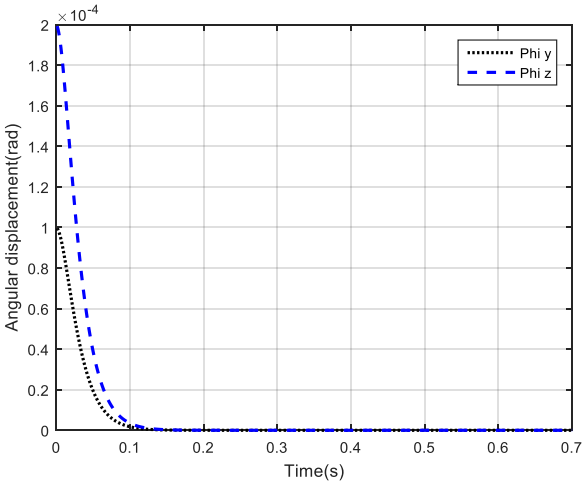

Figure 6. The position of the axis angle θ_y, θ_z.

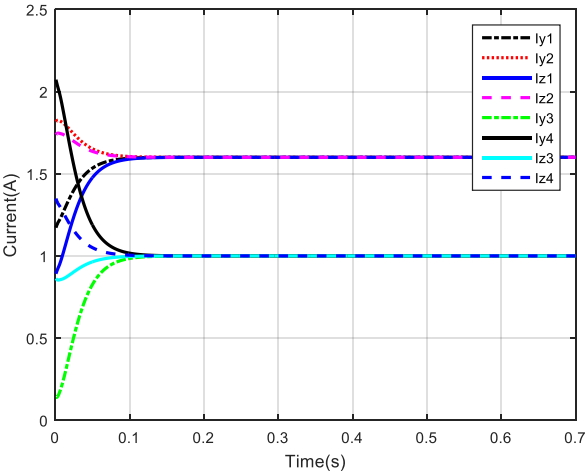

Figure 7. Control current response.

at first to bring the rotor to equilibrium, but once the rotor returns to equilibrium, the force is kept stable at the values F_{01} and F_{02}. From the above results, it can be concluded that the controller is designed to completely satisfy the requirements.

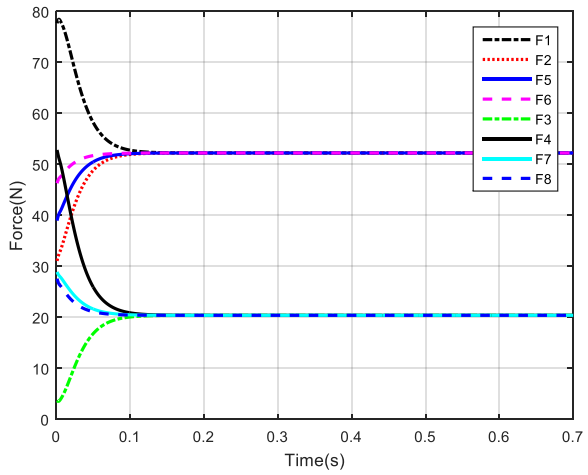

FIGURE 8. Impact force of electromagnets.

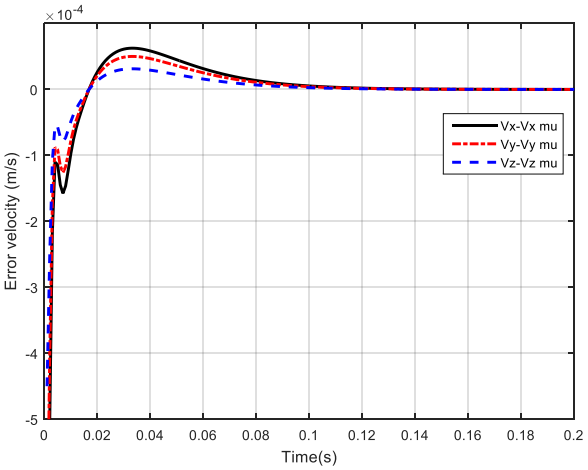

FIGURE 9. Velocity deviation of x, y, z axes according to observer.

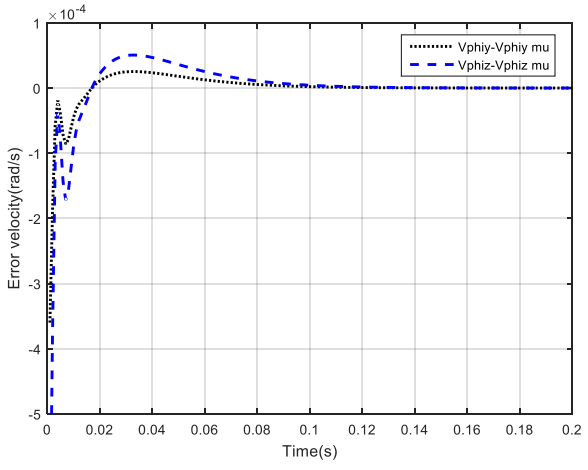

FIGURE 10. Velocity deviation of θ_y, θ_z axes according to observer.

Based on Fig. 9 and Fig. 10, the observer satisfied the requirements, and the estimated velocity values were near to the real velocity value after 0.1 s.

4.2. SIMULATION SCENARIO 2:

The rotor speed will be changed to 12000 rpm to evaluate the controllability of the controller when the rotor is in the high-speed region, the initial value of the rotor's centre of mass is: $x_0 = 0.25.10^{-3}; y_0 = 0.2.10^{-3}; z_0 = 0.125.10^{-3}; \theta_y = 0.1.10^{-3}; \theta_z = 0.2.10^{-3}$.

The simulation results on the x, y, and z axes are identical to the first simulation scenario, as shown in Fig. 12, where the angular position responses of the axes θ_y, θ_z have an undershoot and the response time has been increased to 0.2 seconds. Only the θ_y and θ_z axes are impacted when the rotor rotates at high speeds, but it soon returns to equilibrium. The suggested controller takes into account the rotor speed factor and demonstrates its capacity to function well in the high-speed region.

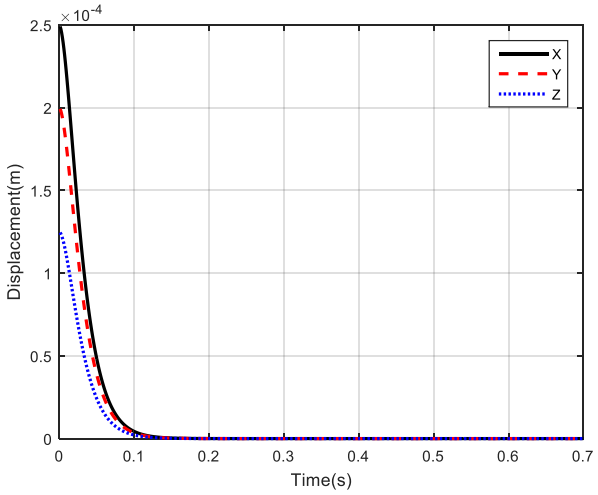

FIGURE 11. Response to the position of the x, y, z axes.

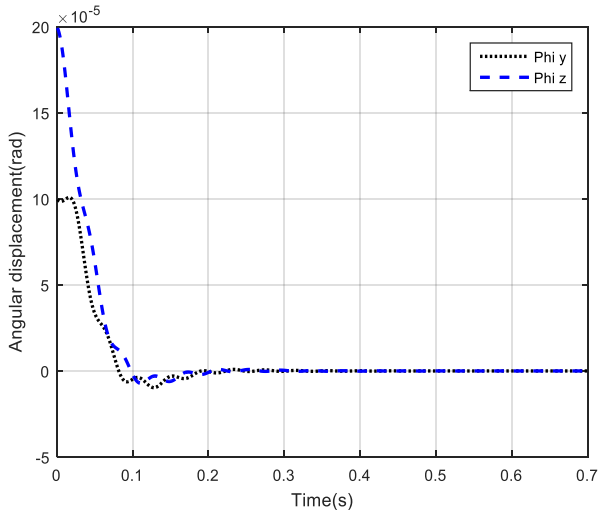

FIGURE 12. The position of the axis angle θ_y, θ_z.

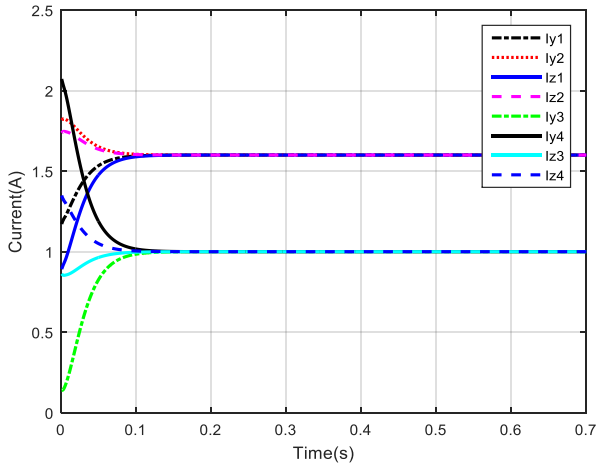

Figure 13. Control current response.

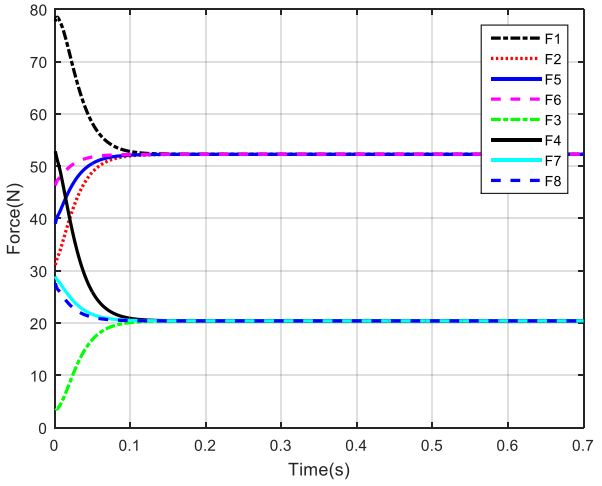

Figure 14. Impact force of electromagnets.

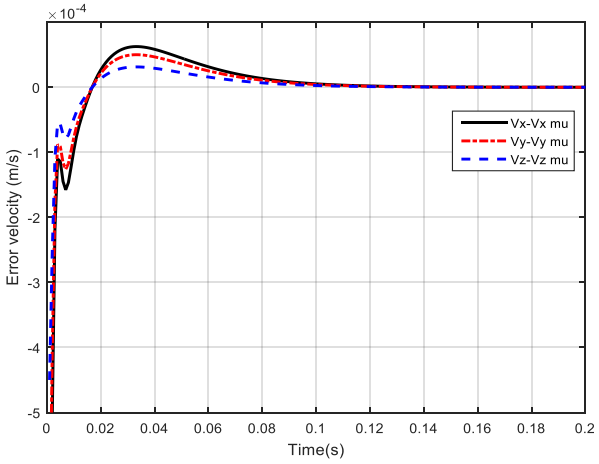

Figure 15. Velocity deviation of x, y, z axes according to observer.

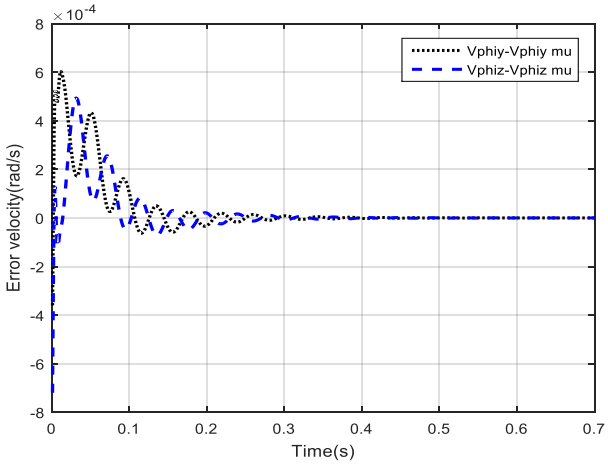

Figure 16. Velocity deviation of θ_y, θ_z axes according to observer.

5. Conclusions

In the paper, we consider the cone-shaped magnetic bearing, which is characterised as a class of under-actuated and strongly coupled systems. Based on control current distribution, the coupling mechanism in electrical sub-system is solved. Subsequently, an active disturbance control is adopted to tackle the rotational-motion-induced disturbance acting on the system. The simulations are carried out proving that the proposed control can effectively bring the the rotor to equilibrium. The results also indicate that the coupling effects from low to high rotational speeds do not have a noticeable impact on the transnational motions of the rotor. In the future, experimental study will be carried out.

Acknowledgements

This research is funded by the Hanoi University of Science and Technology (HUST) under project number T2021-PC-001.

References

[1] C. R. Knospe. Active magnetic bearings for machining applications. *Control Engineering Practice* **15**(3):307–313, 2007. https://doi.org/10.1016/j.conengprac.2005.12.002.

[2] W. Ding, L. Liu, J. Lou. Design and control of a high-speed switched reluctance machine with conical magnetic bearings for aircraft application. *IET Electric Power Applications* **7**(3):179–190, 2013. https://doi.org/10.1049/iet-epa.2012.0319.

[3] P. Imoberdorf, C. Zwyssig, S. D. Round, J. Kolar. Combined radial-axial magnetic bearing for a 1 kW, 500,000 rpm permanent magnet machine. In *APEC 07 - Twenty-Second Annual IEEE Applied Power Electronics Conference and Exposition*, pp. 1434–1440. 2007. https://doi.org/10.1109/APEX.2007.357705.

[4] J. X. Shen, K. J. Tseng, D. M. Vilathgamuwa. A novel compact PMSM with magnetic bearing for artificial heart application. *IEEE Transactions on Industry Applications* **36**(4):1061–1068, 2000. https://doi.org/10.1109/28.855961.

[5] M. D. Noh, S. R. Cho, J. H. Kyung, et al. Design and implementation of a fault-tolerant magnetic bearing

system for turbo-molecular vacuum pump. *IEEE/ASME Transactions on Mechatronics* **10**(6):626–631, 2005. https://doi.org/10.1109/TMECH.2005.859830.

[6] B. Han, S. Zheng, Y. Le, S. Xu. Modeling and analysis of coupling performance between passive magnetic bearing and hybrid magnetic radial bearing for magnetically suspended flywheel. *IEEE Transactions on Magnetics* **49**(10):5356–5370, 2013. https://doi.org/10.1109/TMAG.2013.2263284.

[7] D. H. Nguyen, M. L. Nguyen, T. L. Nguyen. Decoupling Control of a Disc-type Rotor Magnetic Bearing. *The International Journal of Integrated Engineering* **13**(5):247–261, 2021. https://doi.org/10.30880/ijie.2021.13.05.026.

[8] A. H. Slocum. Introduction to Precision Machine Design. *Precision Machine Design* pp. 390–399, 1992.

[9] H. S. Jeong, C. S. Kim. Modeling and Control of Active Magnetic Bearings, 1994.

[10] S. Xu, J. Fang. A Novel Conical Active Magnetic Bearing with Claw Structure. *IEEE Transactions on Magnetics* **50**(5), 2014. https://doi.org/10.1109/TMAG.2013.2295060.

[11] A. Mohamed, F. Emad. Conical magnetic bearings with radial and thrust control. In *Proceedings of the 28th IEEE Conference on Decision and Control*, pp. 554–561. 1989. https://doi.org/10.1109/CDC.1989.70176.

[12] C. W. Lee, H. S. Jeong. Dynamic modeling and optimal control of cone-shaped active magnetic bearing systems. *Control Engineering Practice* **4**(10):1393–1403, 1996. https://doi.org/10.1016/0967-0661(96)00149-9.

[13] J. Fang, C. Wang, J. Tang. Modeling and analysis of a novel conical magnetic bearing for vernier-gimballing magnetically suspended flywheel. *Proceedings of the Institution of Mechanical Engineers, Part C: Journal of Mechanical Engineering Science* **228**(13):2416–2425, 2014. https://doi.org/10.1177/0954406213517488.

[14] S. J. Huang, L. C. Lin. Fuzzy modeling and control for conical magnetic bearings using linear matrix inequality. *Journal of Intelligent and Robotic Systems: Theory and Applications* **37**(2):209–232, 2003. https://doi.org/10.1023/A:1024137007918.

[15] E. E. Ovsyannikova, A. M. Gus'kov. Stabilization of a Rigid Rotor in Conical Magnetic Bearings. *Journal of Machinery Manufacture and Reliability* **49**(1):8–15, 2020. https://doi.org/10.3103/S1052618820010100.

[16] D. H. Nguyen, T. L. Nguyen, M. L. Nguyen, H. P. Nguyen. Nonlinear control of an active magnetic bearing with output constraint. *International Journal of Electrical and Computer Engineering (IJECE)* **8**(5):3666, 2019. https://doi.org/10.11591/ijece.v8i5.pp3666-3677.

[17] D. H. Nguyen, T. L. Nguyen, D. C. Hoang. A non-linear control method for active magnetic bearings with bounded input and output. *International Journal of Power Electronics and Drive Systems* **11**(4):2154–2163, 2020. https://doi.org/10.11591/ijpeds.v11.i4.pp2154-2163.

[18] A. Katyayn, P. K. Agarwal. Type-2 fuzzy logic controller for conical amb-rotor system. In *2017 4th International Conference on Power, Control & Embedded Systems (ICPCES)*, pp. 1–6. 2017. https://doi.org/10.1109/ICPCES.2017.8117616.

[19] J. Han. From PID to active disturbance rejection control. *IEEE Transactions on Industrial Electronics* **56**(3):900–906, 2009. https://doi.org/10.1109/TIE.2008.2011621.

[20] G. Herbst. A simulative study on active disturbance rejection control (ADRC) as a control tool for practitioners. *Electronics* **2**(3):246–279, 2013. https://doi.org/10.3390/electronics2030246.